Isolation and Characterization of the Unexpected 1-n-Octyloxyperopyrene: a Solution-processable p-Type Organic Semi-conductor

Marta Martínez-Abadía,[a] Gabriella Antonicelli,[a] Akinori Saeki,[b] Manuel Melle-Franco,[c] Aurelio Mateo-Alonso*[,a,d]

[a] *POLYMAT, University of the Basque Country UPV/EHU, Avenida de Tolosa 72, E-20018 Donostia-San Sebastian, Spain. E-mail: amateo@polymat.eu*

[b] *Department of Applied Chemistry, Graduate School of Engineering, Osaka University, Suita, Osaka 565-0871, Japan*

[c] *CICECO - Aveiro Institute of Materials, Department of Chemistry, University of Aveiro, 3810-193 Aveiro, Portugal.*

[d] *Ikerbasque, Basque Foundation for Science, Bilbao, Spain.*

ABSTRACT

The synthesis and optical, electrochemical, thermal and electrical characterization of a new and unexpected 1-n-octyloxyperopyrene is reported. The structure of 1-n-octyloxyperopyrene has been unambiguously established by single crystal X-ray diffraction. The solubility of this polycyclic aromatic hydrocarbon, endowed by the alkoxy substituent, allows the fabrication of thin film field-effect transistors by liquid deposition methods. These devices show hole mobilities up to 1.61×10^{-3} cm^2 V^{-1} s^{-1}.

In recent years polycyclic aromatic hydrocarbons (PAHs) have received increasing attention due to their potential applications as semiconducting materials in the area of organic and flexible electronics, including photovoltaic solar cells, organic light emitting diodes and organic field-effect transistors (OFETs).[1-11] The number of fused rings on the aromatic core and their arrangement play an important role on the energy levels and on the packing in the solid state, which in turn affect charge transport properties. Another important aspect is the solubility, which is key to enable large-area low-cost liquid deposition methods.[12]

Along these lines, peropyrene is a PAH constituted of seven fused benzene rings with armchair edges[13-17] that is receiving a lot of interest[18-26] due to its properties with potential in singlet fission,[19] and hole-transporting[25] applications. Even if the first reports on peropyrene dates back to 1960,[13] the properties of its derivatives remain largely unexplored. Herein, we describe the isolation and characterization of a new peropyrene derivative, namely 1-*n*-octyloxyperopyrene (**1**), which has been obtained as an unexpected side-product of a know reaction. The structure of **1** has been unambiguously established by single crystal X-ray diffraction, among other structural characterization techniques. Furthermore, a broad optoelectronic, electrochemical, thermal and electrical study illustrate that peropyrene **1** is a promising thermally-stable solution-processable p-type organic semiconductor.

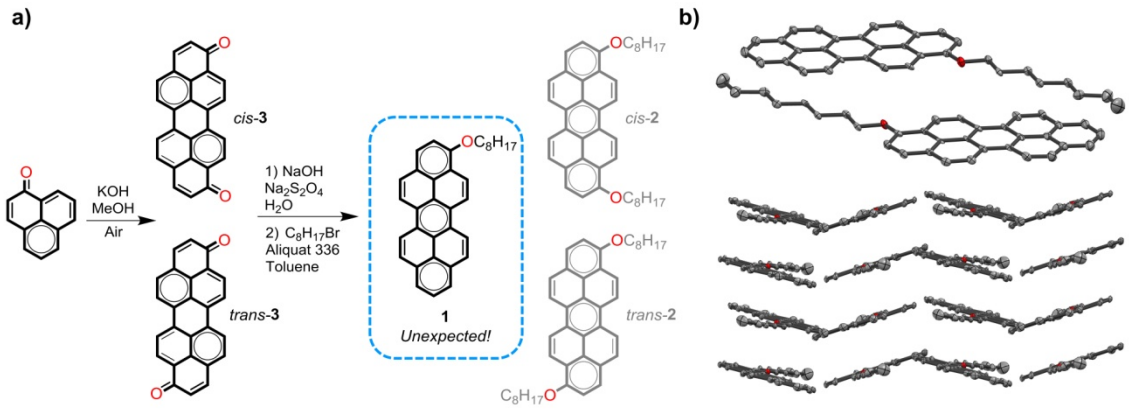

Figure 1 a) Synthetic route to **1**. b) Single crystal structure of **1**. Top: view of each pair showing an antiparallel alignment. Bottom: side-view showing pairwise herringbone packing structure.

Recently, we have reported a new family of low-molecular-weight hole transporting gelators based on peropyrene that can be easily deposited by sol-gel processing.[25] The synthesis of these dialkoxylated peropyrene gelators (a cis and trans isomer mixture of peropyrene **2**, **Figure 1a**) yielded a side-product that we were not able to isolate and characterize at the time. The synthesis proceeds through two steps. In the first step that was previously described by Clar,[13] perinaphtenone is condensed into an unseparable mixture of the cis and trans isomers of peropyrenequinone **3**. The second step[25] involved the ones step reduction of diones to diols using sodium dithionite followed by in-situ alkylation of the alcohols to ethers using *n*-octylbromide. Besides an inseparable mixture of the cis and trans isomers of peropyrene **2** (10% yield) an additional orange compound was isolated by chromatography (2% yield). Orange crystals suitable for X-ray diffraction were obtained from chloroform at room temperature, which showed that the structure of the unknown compound corresponds to the unexpected 1-*n*-octyloxyperopyrene (**1**). Peropyrene **1** crystallizes in the P21/n monoclinic space group (**Figure 1b**) and packs in a herringbone pair motif with an antiparallel alignment of each pair, where the aliphatic chain of one molecule with the aromatic core of an adjacent one (**Figure 1b top**). NMR, MALDI-TOF MS characterization of peropyrene **1** is also consistent with the X-ray structure. A likely rational for the formation of peropyrene **1** could be the overreduction of one of the ketones during the reduction step with sodium dithionite.

Theoretical calculations were performed to gain insight the structure and electronic structure of peropyrene **1**. The geometry was obtained from a simulated annealing MD run in vacuum with a recent tight-binding Hamiltonian.[27] The gas phase DFT calculations yielded a minimum with C_s symmetry and reproduced successfully the

bond alternation found from the experimental single crystal X-ray analysis. The simulations showed the four localized double bonds predicted by Clar's empirical rule[28, 29] (**Figure S3**). The differences are small, up to 0.02 Å, and might be ascribed to small structural distortions in the condensed phase. In fact, while the DFT minimum has a plane of symmetry containing all the carbon atoms the molecule is bent, if slightly, out a planarity in the crystal. Interestingly, the analysis of the crystal structure and DFT calculations confirmed the two aromatic sextets are localized on the two terminal rings. However, the one predicted in the internal ring has clearly larger single character than expected from the Clar's rule,[28, 29] as previously predicted by chemical graph theory.[30] The effect of the chain conformation was also investigated by comparing two conformations, one with an extended aliphatic chain and one with a bent chain, yielding virtually the same results (**Figure S4**).

To investigate the photophysical properties and also to establish the energy levels of peropyrene **1**, absorption and fluorescence spectroscopy and cyclic voltammetry were performed. The electronic absorption spectrum **(Figure 2a)**, in chloroform, shows three sets of bands with distinct vibrational structures typical of peropyrene derivatives.[13, 15] The longest absorption wavelength for compound **1** is 461 nm, which is slightly blue-shifted in comparison to the previously described dialkoxylated peropyrene **2** (471 nm).[25] The fluorescence spectrum for peropyrene **1** exhibits a clear vibronic structure with a maximum at 471 nm **(Figure 2a)**. The voltammogram illustrates peropyrene **1** is an electron-rich PAH, exhibiting only oxidation processes (**Figure 2b**). Two reversible anodic redox waves were observed at +0.23 and +0.74 V versus ferrocene (Fc) that was used as an internal standard.

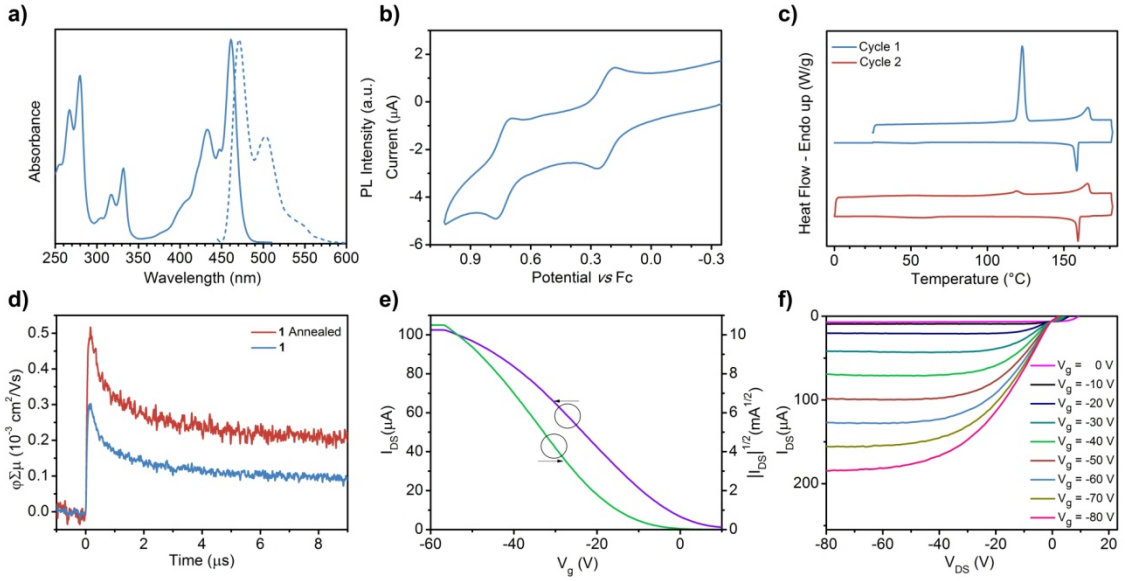

Figure 2 a) Absorption and photoluminescence (dash line) spectra of **1** in chloroform; b) Cyclic voltammograms of **1** in dichloromethane (0.1 M nBu$_4$PF$_6$); c) DSC thermograms at 10 °C min^{-1} for **1**; d) FP-TRMC (λ_{exc} = 355 nm) of the as-obtained powder of **1** (blue line), obtained from chloroform evaporation, or of the annealed powder at 150 °C of **1** (red line). e) Representative transfer and square root of the absolute values of current as a function of gate potential of thin films of **1**; and f) Output curves of thin films of **1**.

The HOMO-LUMO gap of **1** (2.60 eV) was estimated from the onset of the longest wavelength absorption, the electrochemical HOMO level (–4.95 eV) from the onset of the first oxidation process and the LUMO level (–2.35 eV) from the difference between HOMO and HOMO-LUMO gap. The computed (B3LYP/6-311+g(2d,p)) HOMO-LUMO gap is very similar (2.7 eV, see **Table S1**). The computed HOMO (–4.9 eV) and the LUMO (–2.2 eV) energies also correlate well with the experimental values. An analysis of the orbitals shows the HOMO and the LUMO reside on the aromatic moiety and on the oxygen atom of the ether functional group (**Figure S5**). The ether functionality accounts for the small difference in the HOMO and LUMO level energies between this molecule and unfunctionalized peropyrene that has slightly more stable frontier orbitals (**Table S1**).

The thermal stability of peropyrene **1** was studied by thermogravimetric analysis (TGA) under nitrogen, without signs of decomposition up to 325 °C. Differential scanning calorimetry (DSC) and polarized optical microscopy (POM) allowed the observation of a new phase between 122 and 165 °C on heating, compatible with the existence of a liquid crystalline phase (**Figure 2c** and **S7**). The annealing above this thermal transition results in a phase change at room temperature as confirmed by PXRD (**Figure S8)**. In contrast to the reported dialkoxylated peropyrene,[25] compound **1** does not form gels in aliphatic alcohols.

The intrinsic charge transport properties of peropyrene **1** were explored by flash-photolysis time-resolved microwave conductivity (FP-TRMC) ($\varphi\Sigma\mu$, where φ is the product of the quantum yield, and $\Sigma\mu$ is the sum of the charge carrier mobilities). For this purpose, the as-obtained powder (obtained from the chloroform evaporation) and the powder annealed at 150 °C were studied in order to assess if the phase transition

changes described above had any effect on charge transport. The results showed a maximum $\varphi\Sigma\mu$ of 3.0 x 10^{-4} cm^2 V^{-1} s^{-1} from the as-obtained powder samples while the $\varphi\Sigma\mu$ increased upon annealing (150 °C for 15 minutes) to 5.2 x 10^{-4} cm^2 V^{-1} s^{-1} (**Figure 2d**).

To further assess the charge transport properties of peropyrene **1**, FETs incorporating **1** as a semiconducting layer were fabricated and studied. By taking advantage of the solubility of the peropyrene **1**, the semiconducting layer was deposited by spin coating solution of **1** in chloroform on prefabricated bottom-contact bottom-gate transistors with prepatterned Au contacts that had been previously passivated by introducing a monolayer of OTs through a wet process. All devices were prepared and characterized before and after 40 minutes annealing at 150 °C inside a glovebox. The devices showed a typical p-type behavior. Representative output and transfer curves are given in **Figure 2** (e,f). The devices without annealing exhibited hole mobilities (μ_h) with a maximum value of 1.56 × 10^{-4} cm^2 V^{-1} s^{-1}. Remarkably, the values increased when the devices were annealed at 150 °C, exhibiting hole mobilities one order of magnitude higher up to 1.61 × 10^{-3} cm^2 V^{-1} s^{-1} with moderate on/off currents ($I_{on/off}$) in the range of 10^1 (**Table S2**).

To conclude, we have reported the isolation and characterization of the unexpected 1-*n*-octyloxyperopyrene (**1**). The structure of **1** has been unambiguously established by single crystal X-ray diffraction, NMR and MS. The *n*-octyloxy substitution endows peropyrene **1** with a high solubility, which has allowed a detailed optoelectronic, electrochemical and electrical characterization, and also, its incorporation in OFETs by liquid deposition methods. These devices show hole mobilities up to 1.61 × 10^{-3} cm^2 V^{-1} s^{-1} after annealing at 150 °C without further optimization. All the above illustrates that

peropyrene derivatives are stable and solution-processable p-type organic semiconductors.

EXPERIMENTAL SECTION

General: Reagents for synthesis were, if not otherwise specified, purchased from Aldrich, TCI or Acros. Commercial chemicals and solvents were used as received. Column chromatography was carried out using Silica gel 60 (40-60 μm) from Scharlab. Peropyrenequinone **3** was synthesized according to reported procedures.[13]

*Synthesis of peropyrene **1***: A solution of NaOH (4.94 g, 125.93 mmol) in 130 mL of water was stirred at 80 °C under an argon atmosphere for 30 minutes. Then sodium dithionite (0.12 g, 0.695 mmol) and the peropyrenequinone **3** (0.44 g, 1.235 mmol) were added. After 1 hour of reduction, Aliquat 336 (5 mL), 1-bromooctane (2.1 mL) and toluene (30 mL) were added. The resulting mixture was stirred at 90 °C for 24 h. Then it was cooled and poured into water and the organic phase was extracted with dichloromethane. The aqueous phase was washed three times with dichloromethane and the combined organic phases washed with water and brine. After drying the organic phase with anhydrous sodium sulfate and removing the solvent, the purification was performed by column chromatography using petroleum ether/dichloromethane 9:1 as an eluent, affording the compound **1** and **2**. Then, the products were dissolved in chloroform and precipitated with methanol, filtered and washed with methanol and a little amount of petroleum ether. 11.2 mg of peropyrene **1** (2 % yield) and 70 mg of orange peropyrene **2**[25] (9.7 % yield) were obtained. ^{1}H NMR (500 MHz, 1,1,2,2-Tetrachloroethane-d_2,): 9.29 – 9.16 (m, 3H), 9.07 (d, *J* = 9.2 Hz, 1H), 8.85 (d, *J* = 9.4 Hz, 1H), 8.46 – 8.23 (m, 6H), 8.15 (t, *J* = 7.6 Hz, 1H), 7.72 (d, *J* = 8.4 Hz, 1H), 4.46 (t, *J* = 6.5 Hz, 2H), 2.17– 2.07 (m, 2H), 1.78 – 1.69 (m, 2H), 1.60 – 1.37 (m, 8H),

0.98 (t, *J* = 6.8 Hz, 3H). ^{13}C NMR (125 MHz, 1,1,2,2-Tetrachloroethane-d_2): δ 153.67, 131.34, 131.30, 127.68, 127.16, 127.10, 126.23, 126.01, 125.94, 125.93, 125.91, 125.24, 125.14, 124.89, 124.84, 124.56, 124.40, 123.08, 123.04, 122.85, 122.78, 121.75, 121.57, 120.80, 120.24, 109.72, 69.43, 69.43, 31.66, 31.66, 29.45, 29.45, 29.27, 29.08, 29.08, 26.16, 22.48, 22.48, 13.91, 13.91. EM (MALDI-TOF) (m/z): calculated for $C_{34}H_{30}O$: 454.230; found: 454.247 $[M]^+$.

Instrumentation: NMR spectra were recorded on Bruker Avance 500 spectrometer at 298 and 363 K using partially deuterated solvents as internal standards. Matrix Assisted Laser Desorption Ionization (coupled to a Time-Of-Flight analyzer) experiments (MALDI-TOF) were recorded on Bruker REFLEX spectrometer in Polymat by Dr. Antonio Veloso. Absorption and emission spectra were recorded on a Perkin-Elmer Lambda 950 spectrometer, and a LS55 Perkin-Elmer Fluorescence spectrometer, respectively. Electrochemical measurements were carried out on a Princeton Applied Research Parstat 2273 in a 3-electrode single compartment cell with Pt disc working electrode (Ø = 0.5 mm), a platinum wire counter electrode (Ø = 0.5 mm) and a silver wire pseudoreference electrode. The cell and the electrodes were custom made. All the values are quoted versus the redox potential of the ferrocene/ferrocenium couple. The HOMO level was estimated from the potential onset of the first oxidation wave (E_{HOMO} = –4.8 –e(E_{ONSET})), the HOMO-LUMO gap was estimated from the absorption onset of the longest wavelength band and the LUMO was estimated from the difference between the HOMO and the HOMO-LUMO gap. TGA/SDTA 851 Mettler Toledo was used to perform the thermogravimetric analysis (TGA) using a 10 °C min^{-1} heating rate under a nitrogen flow, which was changed to oxygen from 800 °C. DSC3+ Mettler Toledo was used to carry out differential scanning calorimetry (DSC). The sample was

sealed in an aluminium pan, and measured at a scanning rate of 10 °C min^{-1} under a nitrogen flow. X-ray single crystal diffraction experiments were performed by the X-ray diffraction unit of General Services SG-Iker (UPV/EHU) by Dr. Leire San Felices. Intensity data were collected on an Agilent Technologies Super-Nova diffractometer, which was equipped with monochromated Cu kα radiation (λ= 1.54184 Å) and Atlas CCD detector. Measurement was carried out at 150.00(10) K with the help of an Oxford Cryostream 700 PLUS temperature device. Data frames were processed (united cell determination, analytical absorption correction with face indexing, intensity data integration and correction for Lorentz and polarization effects) using the Crysalis software package. The structure was solved using Olex2 and refined by full-matrix least-squares with SHELXL-97. Final geometrical calculations were carried out with Mercury and PLATON as integrated in WinGX. The X-ray powder diffraction experiments were performed by the X-ray diffraction unit of General Services SG-Iker (UPV/EHU) by Dr. Aitor Larrañaga. Patterns were collected by using a PHILIPS X'PERT PRO automatic diffractometer operating at 40 kV and 40 mA, in theta-theta configuration, secondary monochromator with Cu-Kα radiation (λ = 1.5418 Å) and a PIXcel solid state detector (active length in 2θ 3.347°). Data were collected from 1 to 50° 2θ (step size = 0.026 and time per step = 300 s, total time 40 min) at room temperature. A variable divergence slit, giving a constant 4.0 mm area of sample illumination, was used. Laser-flash TRMC experiments were conducted for the sample on a quartz plate using the third harmonic generator (THG; 355 nm) of a Nd:YAG laser (Continuum Inc., Surelite II, 5–8 ns pulse duration, 10 Hz) as the excitation source (9.1 × 10^{15} photons cm^{-2} $pulse^{-1}$). The photoconductivity transient Δσ was converted to the product of the quantum yield (ϕ) and the sum of charge carrier mobilities ∑μ (= μ+ + μ–) by the formula $\phi\sum\mu = \Delta\sigma(eI_0F_{light})^{-1}$, where e

and F_{light} are the unit charge of a single electron and a correction (or filling) factor, respectively.

Fabrication of FET devices: Commercially available interdigital Au electrodes (15x15 mm^2) from Fraunhofer IPM were used for FET fabrication. High doped n-type silicon was used as gate electrode. A 30 nm Au electrode with a 10 nm high work function adhesion layer (ITO) (structured by lift-off technique) was patterned as source and drain electrodes respectively on the gate dielectric of 230 nm thermal-oxidized SiO_2. First, the electrodes were cleaned one by one by ultrasonication with electronic grade acetone and isopropanol and dried under compressed N_2. Then, the electrodes were treated with oxygen plasma for 15 minutes. To form self-assembled monolayers (SAMs) of octadeciltrichlorosilane (OTs) on the SiO_2 surface, the substrates were dipped into a solution of OTs (4 mM) in toluene and heated at 50 °C during 30 minutes. The modified electrodes were subsequently washed with chloroform and dried for 1 hour at 80 °C. Finally, the substrates were cleaned again with electronic grade acetone and isopropanol and dried with N_2. The thin films of compound **1** were deposited by spin coating of solutions in chloroform (5 mg/mL). The electrical characterization of the devices was carried out with a Keithley 2636B semiconductor analyzer system, which connected to a probe-station under nitrogen at room temperature. The mobility of each electrode was calculated in the saturation regime using Equation 1:

$$I_{DS,sat} = \frac{CiW}{2L}\,\mu_{FE}(V_{GS} - V_T) \quad \textbf{Equation 1}$$

Where μ_{FE} is the field-effect mobility, *Ci* is the capacitance per unit area of the dielectric layer, *L* is the channel length, *W* is the channel width, V_T is the threshold voltage and V_{GS} is the gate-source bias.

ACKNOWLEDGMENT

We are grateful to the Basque Science Foundation for Science (Ikerbasque), POLYMAT, the University of the Basque Country (SGIker), Gobierno de España (Ministerio de Economía y Competitividad CTQ2016-77970-R), Gobierno Vasco (BERC program), Diputación Foral de Guipúzcoa (OF215/2016(ES)), the Portuguese Foundation for Science and Technology (IF/00894/2015) and CICECO - Aveiro Institute of Materials, POCI-01-0145-FEDER-007679 (FCT Ref. UID /CTM /50011/2013).

REFERENCES

1. S. Sergeyev, W. Pisula and Y. H. Geerts, *Chem. Soc. Rev.*, 2007, **36**, 1902-1929.
2. J. Wu, W. Pisula and K. Müllen, *Chem. Rev.*, 2007, **107**, 718-747.
3. W. Pisula, X. Feng and K. Müllen, *Chem. Mater.*, 2011, **23**, 554-567.
4. J. Mei, Y. Diao, A. L. Appleton, L. Fang and Z. Bao, *J. Am. Chem. Soc.*, 2013, **135**, 6724-6746.
5. A. Mateo-Alonso, *Chem. Soc. Rev.*, 2014, **43**, 6311-6324.
6. Z. Sun, Z. Zeng and J. Wu, *Acc. Chem. Res.*, 2014, **47**, 2582-2591.
7. M. Ball, Y. Zhong, Y. Wu, C. Schenck, F. Ng, M. Steigerwald, S. Xiao and C. Nuckolls, *Acc. Chem. Res.*, 2015, **48**, 267-276.
8. L. Zhang, Y. Cao, N. S. Colella, Y. Liang, J.-L. Brédas, K. N. Houk and A. L. Briseno, *Acc. Chem. Res.*, 2015, **48**, 500-509.
9. J. T. Markiewicz and F. Wudl, *ACS Appl. Mater. Interfaces*, 2015, **7**, 28063-28085.
10. T. Wöhrle, I. Wurzbach, J. Kirres, A. Kostidou, N. Kapernaum, J. Litterscheidt, J. C. Haenle, P. Staffeld, A. Baro, F. Giesselmann and S. Laschat, *Chem. Rev.*, 2016, **116**, 1139-1241.
11. A. Mateo-Alonso, *Eur. J. Org. Chem.*, 2017, **2017**, 7006-7011.
12. G. Nisato, D. Lupo and S. Ganz, eds., *Organic and Printed Electronics - Fundamentals and Applications*, Pan Standford Publishing, Singapore, 2016.
13. E. Clar, G. S. Fell, C. T. Ironside and A. Balsillie, *Tetrahedron*, 1960, **10**, 26-36.
14. T. Umemoto, T. Kawashima, Y. Sakata and S. Misumi, *Tetrahedron Lett.*, 1975, **16**, 463-466.
15. E. Clar and W. Schmidt, *Tetrahedron*, 1978, **34**, 3219-3224.
16. S. Pogodin and I. Agranat, *Org. Lett.*, 1999, **1**, 1387-1390.
17. L. Beer, S. K. Mandal, R. W. Reed, R. T. Oakley, F. S. Tham, B. Donnadieu and R. C. Haddon, *Cryst. Growth Des.*, 2007, **7**, 802-809.

18. S. Geib, S. C. Martens, M. Märken, A. Rybina, H. Wadepohl and L. H. Gade, *Chem. -Eur. J.*, 2013, **19**, 13811-13822.

19. V. M. Nichols, M. T. Rodriguez, G. B. Piland, F. Tham, V. N. Nesterov, W. J. Youngblood and C. J. Bardeen, *J. Phys. Chem. C*, 2013, **117**, 16802-16810.

20. T. K. Dickens and R. B. Mallion, *J. Phys. Chem. A*, 2015, **119**, 5019-5025.

21. W. Yang, J. H. S. K. Monteiro, A. de Bettencourt-Dias and W. A. Chalifoux, *Can. J. Chem.*, 2016, **95**, 341-345.

22. W. Yang, J. H. S. K. Monteiro, A. de Bettencourt-Dias, V. J. Catalano and W. A. Chalifoux, *Angew. Chem., Int. Ed.*, 2016, **55**, 10427-10430.

23. W. Yang and W. A. Chalifoux, *Synlett*, 2017, **28**, 625-632.

24. K. Uchida, T. Kubo, D. Yamanaka, A. Furube, H. Matsuzaki, R. Nishii, Y. Sakagami, A. Abulikemu and K. Kamada, *Can. J. Chem.*, 2017, **95**, 432-444.

25. M. Martinez-Abadia, G. Antonicelli, A. Saeki and A. Mateo-Alonso, *Angew. Chem., Int. Ed.*, 2018, **57**, 8209-8213.

26. W. Yang, R. R. Kazemi, N. Karunathilake, V. J. Catalano, M. A. Alpuche-Aviles and W. A. Chalifoux, *Org. Chem. Front.*, 2018, **5**, 2288-2295.

27. S. Grimme, C. Bannwarth and P. Shushkov, *J. Chem. Theory Comput.*, 2017, **13**, 1989-2009.

28. E. Clar, *Polycyclic Hydrocarbons*, Academic, London, 1964.

29. E. Clar, *The Aromatic Sextet*, Wiley, New York, NY, 1972.

30. M. Randić and A. T. Balaban, *Int. J. Quantum Chem.*, 2018, **118**, e25657.